AD

TECHNICAL REPORT ARCCB-TR-99014

THERMOCHEMICAL MODEL OF HYDROGEN CRACKING AT HEAT-AFFECTED CANNON BORE SURFACES

J. H. UNDERWOOD
G. N. VIGILANTE
E. TROIANO

AUGUST 1999

US ARMY ARMAMENT RESEARCH,
DEVELOPMENT AND ENGINEERING CENTER
CLOSE COMBAT ARMAMENTS CENTER
BENÉT LABORATORIES
WATERVLIET, N.Y. 12189-4050

APPROVED FOR PUBLIC RELEASE; DISTRIBUTION UNLIMITED

DISCLAIMER

The findings in this report are not to be construed as an official Department of the Army position unless so designated by other authorized documents.

The use of trade name(s) and/or manufacturer(s) does not constitute an official endorsement or approval.

DESTRUCTION NOTICE

For classified documents, follow the procedures in DoD 5200.22-M, Industrial Security Manual, Section II-19, or DoD 5200.1-R, Information Security Program Regulation, Chapter IX.

For unclassified, limited documents, destroy by any method that will prevent disclosure of contents or reconstruction of the document.

For unclassified, unlimited documents, destroy when the report is no longer needed. Do not return it to the originator.

REPORT DOCUMENTATION PAGE

Form Approved
OMB No. 0704-0188

1. AGENCY USE ONLY *(Leave blank)*	2. REPORT DATE	3. REPORT TYPE AND DATES COVERED
	August 1999	Final

4. TITLE AND SUBTITLE

THERMOMECHANICAL MODEL OF HYDROGEN CRACKING AT HEAT-AFFECTED CANNON BORE SURFACES

5. FUNDING NUMBERS

PRON No. 99797WR00542

6. AUTHOR(S)

J.H. Underwood, G.N. Vigilante, and E. Troiano

7. PERFORMING ORGANIZATION NAME(S) AND ADDRESS(ES)

U.S. Army ARDEC
Benet Laboratories, AMSTA-AR-CCB-O
Watervliet, NY 12189-4050

8. PERFORMING ORGANIZATION REPORT NUMBER

ARCCB-TR-99014

9. SPONSORING / MONITORING AGENCY NAME(S) AND ADDRESS(ES)

U.S. Army ARDEC
Close Combat Armaments Center
Picatinny Arsenal, NJ 07806-5000

10. SPONSORING / MONITORING AGENCY REPORT NUMBER

11. SUPPLEMENTARY NOTES

Presented at the International Workshop on Hydrogen Management for Welding Applications, Ottawa, Canada, 6-8 October 1998. Published in proceedings of the workshop.

12a. DISTRIBUTION / AVAILABILITY STATEMENT

Approved for public release; distribution unlimited.

12b. DISTRIBUTION CODE

13. ABSTRACT *(Maximum 200 words)*

Two examples of hydrogen cracking in the heat-affected region of fired cannons are given, including metallographic evidence of damage at various depths near the bore surface. The depth of steel transformation due to firing is used to verify near-bore temperature distributions and transient and residual stress distributions calculated using classic one-dimensional heat flow analysis. Predicted depths of thermal damage and hydrogen cracks compare well with observed depths for different crack orientations and firing temperatures. Laboratory fracture mechanics tests using bolt-load compact specimens are described, including crack growth and blunt-notched tests in acid-hydrogen environments. The utility of the thermal and fracture mechanics analyses and the laboratory fracture mechanics tests used with cannons are discussed for weld applications.

14. SUBJECT TERMS

Thermomechanical Model, Cannon Bore, Thermal Stress, Hydrogen Cracking, Fracture Mechanics

15. NUMBER OF PAGES

15

16. PRICE CODE

17. SECURITY CLASSIFICATION OF REPORT	18. SECURITY CLASSIFICATION OF THIS PAGE	19. SECURITY CLASSIFICATION OF ABSTRACT	20. LIMITATION OF ABSTRACT
UNCLASSIFIED	UNCLASSIFIED	UNCLASSIFIED	UL

TABLE OF CONTENTS

TABLES

LIST OF ILLUSTRATIONS

ACKNOWLEDGEMENTS

We are pleased to acknowledge the help of colleagues at Benet Laboratories, including the metallographic characterization work of Mr. C. Rickard and the helpful discussions with Dr. S. Sopok and Dr. P. Vottis.

INTRODUCTION

Experience with hydrogen cracking of cannon components has prompted metallographic and fractographic characterization of the cracking events (refs 1-3), laboratory measurement of hydrogen cracking resistance of cannon steels (refs 4,5), and modeling of the thermal stresses that can drive the cracks (ref 3). The cracking of broadest interest occurs at the heat-affected bore surface of a cannon as a result of firing modern high-temperature rounds. The transient thermal firing stresses are often so high in compression that significant yielding occurs, resulting in residual tensile stresses that drive the hydrogen cracks.

The objective here is to compare the thermal damage, hydrogen cracking, and thermal stress model results for two series of cannon firings, one with very high combustion gas temperature (3820°K) and the other with a moderately high gas temperature (3000°K). Metallographic measurements of depths of damage and cracking for the two temperatures compared with those predicted from the thermomechanical model will help understand and control hydrogen cracking in heat-affected areas of cannons. Some of these methods may also be used to control hydrogen cracking in weldments, where the materials and the concerns with heat-affected areas and thermal stresses are often similar to those in cannon applications.

HYDROGEN CRACKING IN CANNONS

Prior Examples; Mechanical Stresses

Two instances of hydrogen cracks that were driven by mechanical stresses in cannon components demonstrate just how serious a concern it can be for the high-strength martensitic steels typically used in cannons. See Table 1. Both examples involved ASTM A723 pressure vessel steel in the 1100 to 1200 MPa strength range, often used for cannons. In the first example (ref 1), tensile overstrain residual stress concentrated at a notch on the outer surface of a cannon tube, combined with acid exposure during a plating operation. This resulted in an astounding 1.7-m long crack in a few minutes, even though there was no cannon firing or other applied loads. The second example (ref 2) showed that cannon component assembly stresses and exposure to firing gases can combine to produce 50-mm long hydrogen cracks after about twenty firings. In both examples, scanning electron fractographs revealed classic intergranular fracture typical of environmental cracking, and the rapid and extensive cracking could not be explained by other fracture mechanisms. Thus, the extreme risk of hydrogen cracking has been clearly demonstrated for cannon components.

Table 1. Examples of Rapid Hydrogen Cracking in Cannons

Material; Yield Strength	Firings; Exposure Time	Crack Growth	Reference
ASTM A723; 1207 MPa	None; ~30 minutes	1700 mm	1
ASTM A723; 1160 MPa	7; ~7 minutes	50 mm	2

Current Examples; Thermal Stresses

Recent work (ref 3) has shown both experimentally and with a thermomechanical model that the heat-affected layer at the bore of a fired cannon can be the site of hydrogen cracking. Metallographic results from this recent work (cannon A) are compared here with similar results from the same type of cannon in which the rounds fired had a significantly lower gas temperature (cannon B). Photomicrographs from the two series of tests are shown in Figures 1 and 2, and key test conditions and average results are summarized in Table 2. Material and configuration characteristics common to all results discussed are: ASTM A723 Grade 2 pressure vessel steel with 1100 MPa yield strength; 60-mm inner radius, 135-mm outer radius; overstrain to a point 50 percent through the wall thickness.

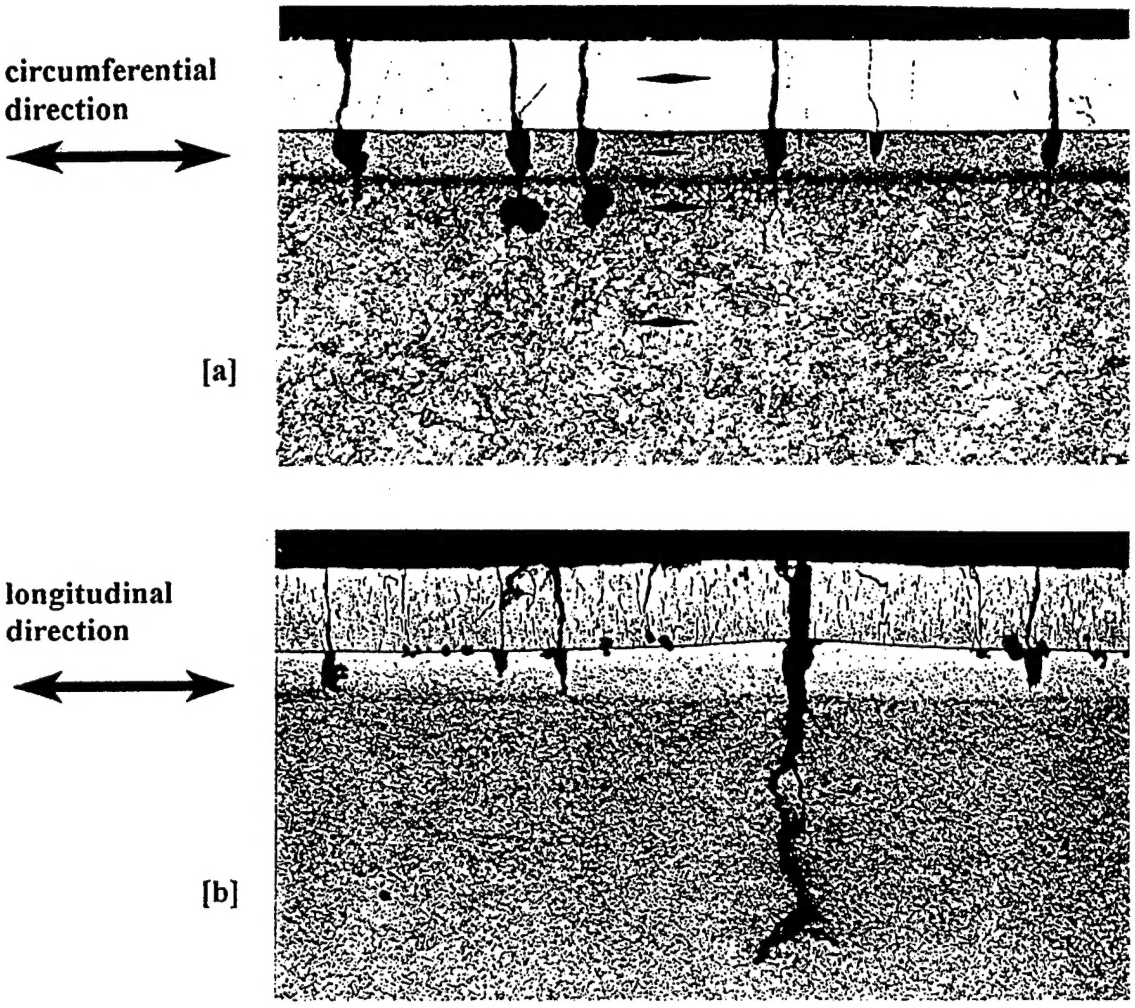

Figure 1. Polished and etched sections from near-bore region of cannon A following 40 firings (100X). Figure 1(a) shows C-R cracks, the steel microstructure, and microhardness indentations. Figure 1(b) shows L-R cracks and the chromium microstructure.

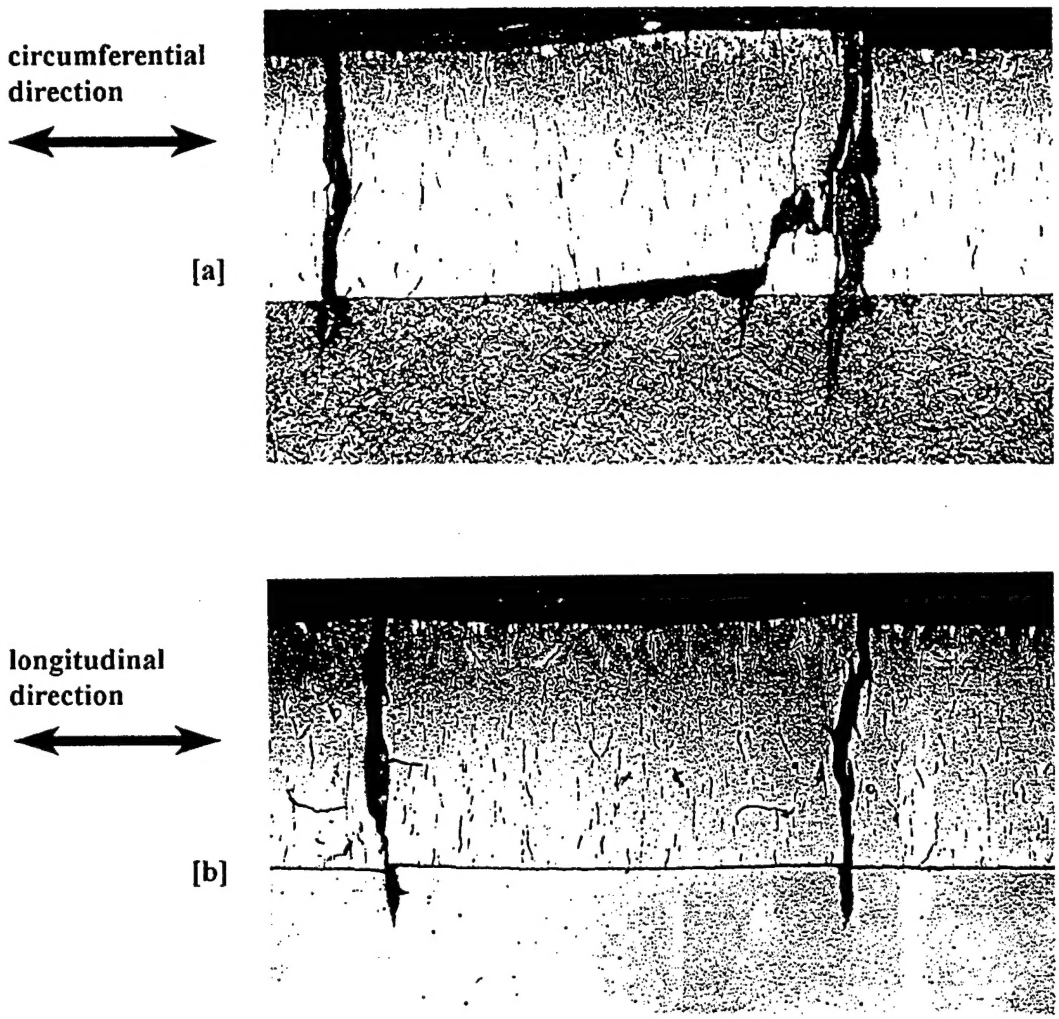

Figure 2. Polished and etched sections from near-bore region of cannon B following 200 firings (200X).
Figure 2(a) shows C-R cracks and the steel and chromium microstructure.
Figure 2(b) shows L-R cracks and the chromium microstructure.

Table 2. Metallographic Characterization of Thermal Damage and Cracking in Cannons

Cannon: Gas Temperature	Number of Firings	Depth of Steel Transformation	Depth of Chromium Recrystallization	Crack Depth
A: 3820°K	~40	0.19 mm	0.08 mm	C-R: 0.23 mm L-R: 0.46 mm
B: 3000°K	~200	None	0.03 mm	C-R: 0,27 mm L-R: 0.29 mm

Figure 1(a) shows the three features typical of cannon A:

- A chromium plated coating (top of photo) to a depth of 0.12-mm
- A layer of thermally transformed untempered martensite to a total depth of 0.19-mm
- The unaffected A723 steel

Note also the microhardness indentations showing a hard transformed layer, as expected, and a chromium hardness about the same as the unaffected steel, which indicates that it has been thermally softened compared to as-plated chromium. Cracks in the C-R orientation (that is, cracks in the plane normal to the circumferential direction, growing in the radial direction) proceed through the chromium layer and into the steel to a depth about equal to the chromium thickness. Figure 1(b) shows cracks in the L-R orientation, with a maximum depth of about twice that of C-R cracks. This may be due to the fact that there is a significant compressive residual stress due to overstrain that serves to limit the depth of C-R cracks. In addition, the chromium microstructure changes noticeably at about two-thirds through the layer, indicating that the temperature reached a characteristic recrystallization temperature (ref 3) at this depth.

The results in Figure 2(a) indicate that cannon B has been much less affected by firing than cannon A, as would be expected because of the lower gas temperature. There is no sign of transformed steel, much less indication of recrystallized chromium, and shallower cracks. (It should be noted here that there are signs of removal of the chromium coating, which is the subject of other investigations.) Table 2 compares key representative results from the metallographic characterization of the two cannons obtained from a series of photomicrographs, including those in Figures 1 and 2. Although cannon B had five times the number of firings, the lower gas temperature of the firings resulted in a lesser degree of thermal effects in each of the three categories. These results will be used to perform checks on the thermomechanical modeling described in the following section. The depth of steel transformation and chromium recrystallization will be used to check the calculated temperature distributions, and the depth of cracks will be used to check the calculated thermal residual stress distributions.

THERMOMECHANICAL MODEL

The basis of the temperature distribution and thermal stress distribution calculations is classic one-dimensional heat flow analysis available in texts on heat transfer, such as Incropera and DeWitt (ref 6) used here. Their closed-form expression for surface convection heat flow for a semi-infinite solid is

$$[T\{x,t\} - T_i]/[T_{gas} - T_i] = erfc[x/2(\beta t)^{1/2}] - [exp[hx/k + h^2\,\beta t/k^2]]$$

$$\times [erfc[x/2(\beta t)^{1/2} + h(\beta t)^{1/2}/k]] \qquad (1)$$

where

$T\{x,t\}$ is the transient temperature distribution for any point, x, below the surface and any time, t.
T_i is the initial temperature of the solid.
T_{gas} is the temperature of the gas.
erfc is the complementary Gaussian error function.
β is thermal diffusivity (m^2/s).
h is thermal convection coefficient (W/m^2K).
k is thermal conductivity (W/mK).

The expression for the biaxial transient thermal stress, S_T, in the plane parallel to the bore surface for temperature $T\{x,t\}$ is (ref 3)

$$S_T = E\alpha[T\{x,t\} - T_i]/[1 - \nu] \qquad (2)$$

where

E is elastic modulus (MPa).
α is thermal expansion coefficient ($1/K$).
ν is Poisson's ratio.

It is interesting to note that equation (2) is identical to the expression that Evans and Hutchinson (ref 7) use to describe the biaxial thermal misfit stress at the interface between layers, except that they use a $\Delta\alpha$ as the mismatch in thermal expansion between layers.

Calculation of biaxial thermal residual stress, $S_{T\text{-}R}$, at and near the bore surface uses equations (1) and (2) and the conventional linear-unloading calculation, as follows:

$$S_{T\text{-}R} = 0 \qquad \text{for } S_T < S_Y$$

$$S_{T\text{-}R} = S_T + S_Y \qquad \text{for } S_T > S_Y \qquad (3)$$

where S_Y is the yield strength of the solid, gun steel in this case.

The most reliable calculations of temperatures and stresses using equations (1) through (3) are in regions where stresses are not much above the yield strength of the material. As seen in the upcoming results, thermal stresses in the region very near the bore surface greatly exceed the yield strength for typical cannon firing conditions. Thus, the model results in the region farther below the bore surface, where thermal stresses are on the order of the yield strength of gun steel, are more reliable. Fortunately, the farthest extent of cracking is the region of primary interest, so the limitation to yield-level stresses is not critical.

MODEL RESULTS

Model calculations were made for the two cannon firing conditions discussed earlier in relation to Table 2. Figure 3 shows temperature-time plots at various depths below the bore surface for the maximum gas temperature of 3820°K for cannon A. The decrease in gas temperature with time shown by the T-gas plot in Figure 3 is based on the known variation of gas temperature during firing described by Sopok et al. (ref 8). The plots at various depths were calculated using equations (1) through (3) and the following thermal and physical properties for steel:

$T_i = 300°K$
$\beta = 6.38\ E - 06\ m^2/s$
$k = 34.5\ W/mK$
$h = 400{,}000\ W/m^2K$
$E = 207{,}000$ MPa
$\alpha = 12\ E - 06\ 1/K$
$\nu = 0.3$
$S_Y = 1100$ MPa

The T_i used was a typical cannon-ambient temperature; the β and k values were for 800°K (ref 6), a representative elevated temperature between T_i and the very high temperatures near the bore; and the E, α, ν, and S_Y values were for room temperature. The h value was selected as 400,000 W/m^2K in order to match the 1022°K steel transformation temperature at the 0.19-mm depth observed from metallographic results. Note that the calculated temperature in Figure 3 for 0.19-mm matches the steel transformation temperature. This value of $h = 400{,}000\ W/m^2K$ was treated as an effective average value and was used for all the calculations discussed here. There is also quite good agreement between the observed depth of chromium recrystallization at 1322°K, 0.08-mm, and the predicted depth from the calculated temperature-time plots, about 0.09-mm. So, using the h value that gives good agreement for the steel transformation also results in good agreement for the chromium recrystallization.

Additional calculations such as those summarized in Figure 3 were made at various temperatures, and the associated maximum temperatures were used to calculate residual stress using equation (3). The maximum temperature and residual stress results are summarized in Figure 4. The point at which the residual stress is zero, at 0.50-mm depth, corresponds to the temperature at which the transient thermal stress is equal to the yield strength of the steel. Note that this point is in good agreement with the observed maximum crack depth, 0.46-mm. Thus, it appears that the hydrogen cracks grew to about the maximum depth of the thermally-generated tensile residual stresses, which is the expected behavior for hydrogen cracks.

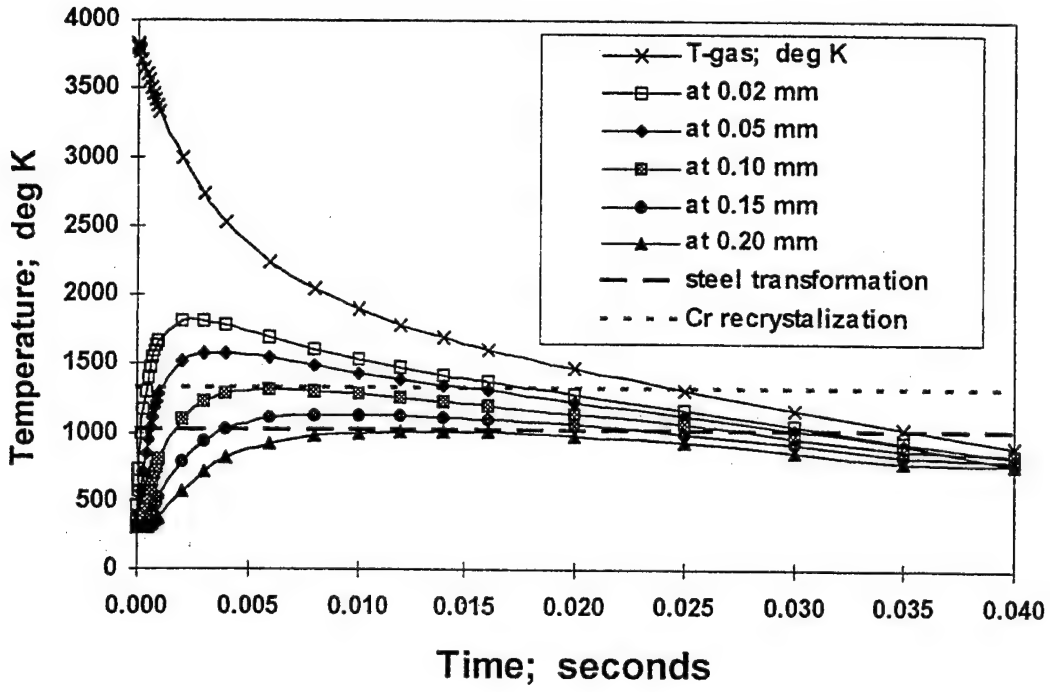

Figure 3. Temperature-time-depth calculations for near-bore region of cannon A using 3820°K maximum gas temperature.

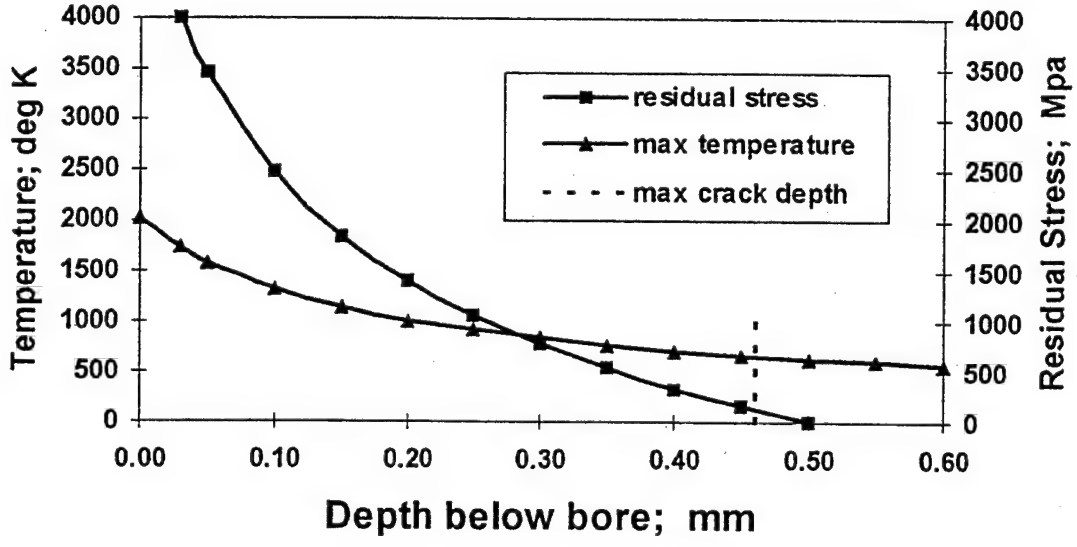

Figure 4. Maximum temperature and thermal residual stress calculations for cannon A using 3820°K maximum gas temperature.

The thermomechanical model results for cannon B with a 3000°K maximum gas temperature are shown in Figures 5 and 6, using all the same input parameters discussed earlier. The predicted steel transformation in Figure 5 is at 0.10-mm depth, which is consistent with the observation that no transformation was seen at the chromium/steel interface, 0.17-mm deep in the case of cannon B. In this case, the chromium layer is effective in preventing transformation of the underlying steel. The predicted depth of chromium recrystallization, 0.04-mm, is close to the 0.03-mm observation. In Figure 6 there is reasonable agreement between the depth for zero calculated residual stress, 0.38-mm, and the maximum observed depth of cracks, 0.29 mm.

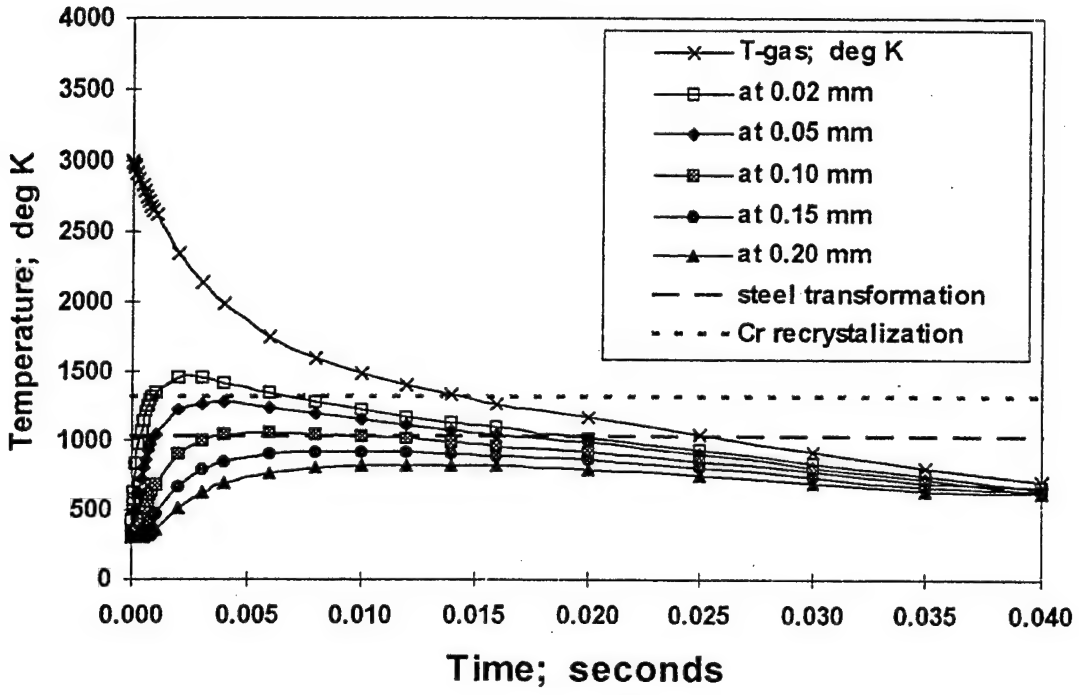

Figure 5. Temperature-time-depth calculations for near-bore region of cannon B using 3000°K maximum gas temperature.

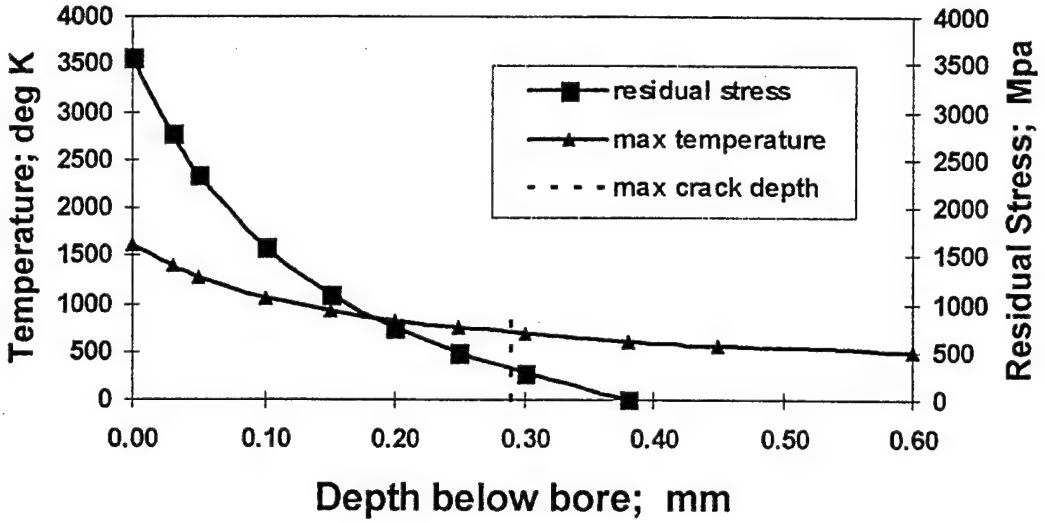

Figure 6. Maximum temperature and thermal residual stress calculations for cannon B using 3000°K maximum gas temperature.

The general conclusion from the above comparisons of model and metallographic results for the near-bore region of fired cannons with two significantly different gas temperatures is that there is general consistency in three independent measures of thermal damage:

- Depth of steel transformation
- Depth of chromium recrystallization
- Depth of hydrogen cracks

By selecting the convection coefficient that matches the predicted depth with the calculated depth of steel transformation for the higher gas temperature, the results for all other comparisons at both gas temperatures are good. Thus, this thermomechanical model has potential use in cannon applications, specifically for the integrated design of the type of steel and thermal barrier coating used with the cannon tube and the propellant combustion gas temperatures used in firing the cannon. The model here is simple enough to be easily accessible compared with the finite difference calculations in prior work (ref 3). It has the disadvantage of using a single constant value of the various material properties to represent a range of temperatures and two different materials. Nevertheless, the model appears to describe the important features of heat-affected cannon surfaces.

LABORATORY HYDROGEN CRACKING TESTS

Experience with hydrogen cracking in cannons has prompted the development of laboratory fracture mechanics tests to measure the resistance to hydrogen cracking in cannon steels (refs 4,5). Current work by Troiano et al. (ref 9) takes a further step to measure resistance to hydrogen cracking of steels with protective coatings, including electrodeposited chromium and nickel and electroless nickel coatings. A brief summary of some of this work is given here.

The test configuration used for much of our laboratory work in hydrogen cracking resistance is the bolt-load compact configuration with a fatigue precrack shown in Figure 7. It has been used for a variety of high-strength steels with current or potential cannon application. The bolt-load compact specimen with a blunt notch is being developed to provide the convenient self-loaded feature of the standard bolt-load specimen, but with a coated notch radius subjected to a known stress to test the cracking resistance of coatings used in cannon applications. Stress calculations have been made for various configurations. Further information on the bolt-load coating tests and results is included in Reference 9.

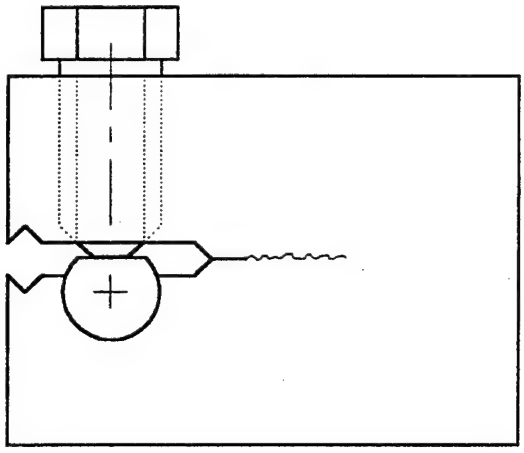

Figure 7. Bolt-load compact specimen used for environmentally-assisted crack growth rate measurements of cannon steels.

Figure 8 shows crack growth rate measurements as a function of applied K in an acid-hydrogen environment for ASTM A723 steel over a range of yield strength (ref 5). The unaffected yield strength of cannons A and B corresponds to the lowest crack growth rates shown, whereas a 20 percent increase in strength results in a three hundred-fold increase in growth rate. A strength increase can occur by the thermal transformation discussed earlier in relation to Figure 1 or by a change in cannon design to decrease weight or increase allowed firing pressure. Regardless of the reason for an increase in yield strength, the result will be the same—a very significant increase in the rate of hydrogen cracking.

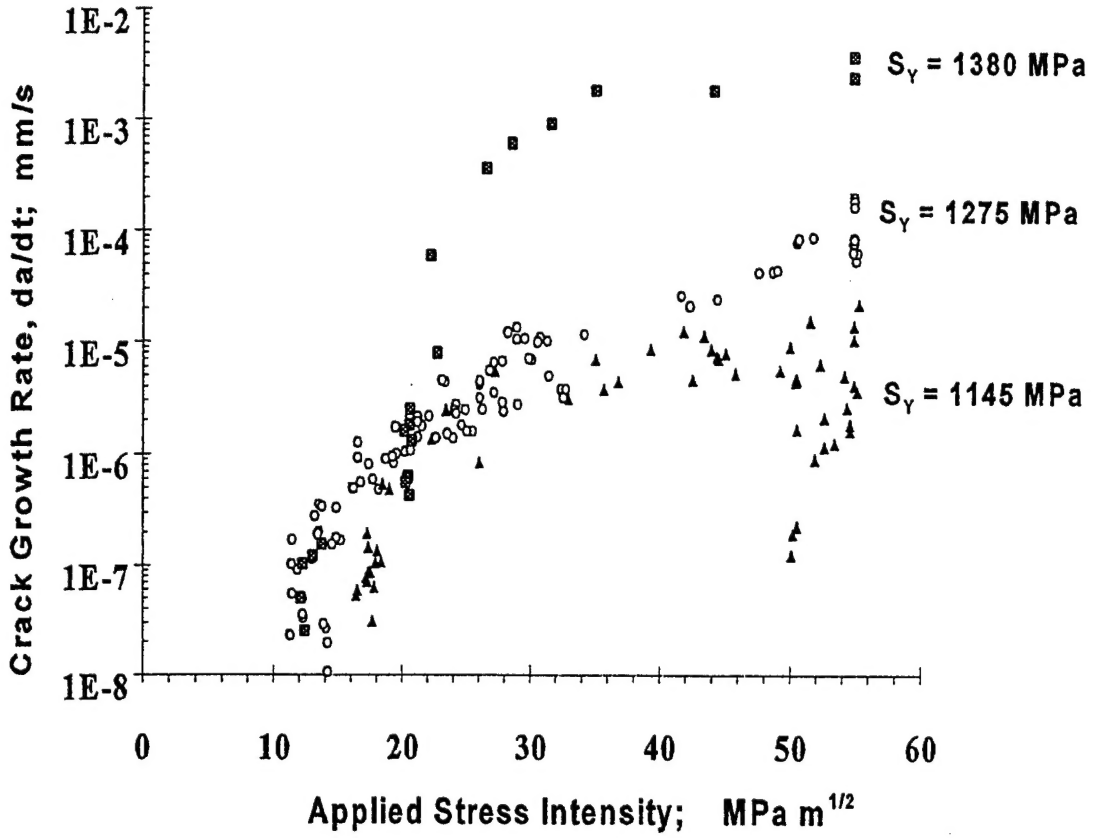

Figure 8. Environmentally-assisted crack growth rate measurements for ASTM A723 steel in concentrated sulfuric/phosphoric acid environment.

CONCLUDING REMARKS

The thermomechanical analysis described here has important use in cannons, to help understand the interactions between the steel and its thermal barrier coating and the hot combustion gas. Thermal damage and transformations in cannons can be well described and in fact, can be used to help verify the residual stress calculations from the thermomechanical model.

Weldments have many basic similarities to cannon bore surfaces, including hot gases and heat-affected zones. So the methods described here for cannons may also be useful for weldments. Residual stresses often have important control over the structural behavior of welds, but values of residual stress are often only estimated as about equal to a material yield strength. The type of model described here can be used to calculate weld residual stresses, and the model and calculations can be verified by metallographic observations, as with the cannon results. Welds, unlike a cannon bore, are not often amenable to simple one-dimensional heat flow analysis. Thus, efficient closed-form analysis as was used for cannons would be limited to relatively simple weld configurations. However, at least for the simple configurations, the advantages of a model to describe the extent of thermal damage and the distribution of residual stress would help considerably in the structural analysis of weldments.

REFERENCES

1. Underwood, J.H., Olmstead, V.J., Askew, J.C., Kapusta, A.A., and Young, G.A., "Environmentally Controlled Fracture of an Overstrained A723 Steel Thick-Wall Cylinder," *Fracture Mechanics: Twenty-Third Symposium, ASTM STP 1189,* (Ravinder Chona, Ed.), American Society for Testing and Materials, Philadelphia, 1993, pp. 443-460.

2. Underwood, J.H., Troiano, E., Vigilante, G.N., Kapusta, A.A., and Tauscher, S., "Hydrogen Cracking During Service of High Strength Steel Cannon Components," *Fatigue and Fracture Mechanics: 29th Volume, STP 1332,* (T.L. Panontin and S.D. Sheppard, Eds.), American Society for Testing and Materials, 1998.

3. Underwood, J.H., Parker, A.P., Cote, P.J., and Sopok, S., "Compressive Thermal Yielding Leading to Hydrogen Cracking in a Fired Cannon," *Fatigue, Fracture, and High Temperature Design Methods in Pressure Vessels and Piping, PVP-Vol. 365,* American Society of Mechanical Engineers, 1998, pp. 293-301.

4. Vigilante, G.N., Underwood, J.H., Crayon, D., Tauscher, S., Sage T., and Troiano, E., "Hydrogen-Induced Cracking Tests of High Strength Steels and Nickel-Iron Base Alloys Using the Bolt-Loaded Specimen," *Fatigue and Fracture Mechanics: 28th Volume, ASTM STP 1321*, American Society for Testing and Materials, 1997, pp. 602-616.

5. Vigilante, G.N., Underwood, J.H., and Crayon, D., "Use of the Instrumented Bolt and Constant Displacement Bolt-Loaded Specimen to Mearure In-Situ Hydrogen Crack Growth in High Strength Steels," *Fatigue and Fracture Mechanics: 30th Volume, ASTM STP 1360*, American Society for Testing and Materials, to be published.

6. Incropera, F.P., and DeWitt, D.P., *Introduction to Heat Transfer,* Wiley, New York, 1985, pp. 202-205; 669-670.

7. Evans A.G., and Hutchinson, J.W., *Acta Metallurgica Materials*, Vol. 43, No. 7, 1995, pp. 2507-2530.

8. Sopok, Samuel; O'Hara, Peter; Pflegl, George; Rickard, Christopher; Vottis, Patrick; and Loomis, Richard, "Erosion Modeling of the 120-mm M256/M829A2 Gun System," *Proceedings of the 1997 ADPA Gun and Ammunition Symposium*, San Diego, April 1997.

9. Troiano, E., Vigilante, G.N., Underwood J.H., and Mossey, C., "Analysis and Recommendations for a Piston Experiencing Environmentally-Assisted Cracking as a Result of Compressive Overloading," presented at the Eighth International Conference on Mechanical Behaviour of Materials, 16-21 May 1999, Victoria, BC, Canada.

TECHNICAL REPORT INTERNAL DISTRIBUTION LIST

	NO. OF COPIES
TECHNICAL LIBRARY ATTN: AMSTA-AR-CCB-O	5
TECHNICAL PUBLICATIONS & EDITING SECTION ATTN: AMSTA-AR-CCB-O	3
OPERATIONS DIRECTORATE ATTN: SIOWV-ODP-P	1
DIRECTOR, PROCUREMENT & CONTRACTING DIRECTORATE ATTN: SIOWV-PP	1
DIRECTOR, PRODUCT ASSURANCE & TEST DIRECTORATE ATTN: SIOWV-QA	1

NOTE: PLEASE NOTIFY DIRECTOR, BENÉT LABORATORIES, ATTN: AMSTA-AR-CCB-O OF ADDRESS CHANGES.

TECHNICAL REPORT EXTERNAL DISTRIBUTION LIST

	NO. OF COPIES
DEFENSE TECHNICAL INFO CENTER ATTN: DTIC-OCA (ACQUISITIONS) 8725 JOHN J. KINGMAN ROAD STE 0944 FT. BELVOIR, VA 22060-6218	2
COMMANDER U.S. ARMY ARDEC ATTN: AMSTA-AR-WEE, BLDG. 3022 AMSTA-AR-AET-O, BLDG. 183 AMSTA-AR-FSA, BLDG. 61 AMSTA-AR-FSX AMSTA-AR-FSA-M, BLDG. 61 SO AMSTA-AR-WEL-TL, BLDG. 59 PICATINNY ARSENAL, NJ 07806-5000	1 1 1 1 1 2
DIRECTOR U.S. ARMY RESEARCH LABORATORY ATTN: AMSRL-DD-T, BLDG. 305 ABERDEEN PROVING GROUND, MD 21005-5066	1
DIRECTOR U.S. ARMY RESEARCH LABORATORY ATTN: AMSRL-WM-MB (DR. B. BURNS) ABERDEEN PROVING GROUND, MD 21005-5066	1
COMMANDER U.S. ARMY RESEARCH OFFICE ATTN: TECHNICAL LIBRARIAN P.O. BOX 12211 4300 S. MIAMI BOULEVARD RESEARCH TRIANGLE PARK, NC 27709-2211	1
COMMANDER ROCK ISLAND ARSENAL ATTN: SIORI-SEM-L ROCK ISLAND, IL 61299-5001	1
COMMANDER U.S. ARMY TANK-AUTMV R&D COMMAND ATTN: AMSTA-DDL (TECH LIBRARY) WARREN, MI 48397-5000	1
COMMANDER U.S. MILITARY ACADEMY ATTN: DEPT OF CIVIL & MECH ENGR WEST POINT, NY 10966-1792	1
U.S. ARMY AVIATION AND MISSILE COM REDSTONE SCIENTIFIC INFO CENTER ATTN: AMSAM-RD-OB-R (DOCUMENTS) REDSTONE ARSENAL, AL 35898-5000	2
COMMANDER U.S. ARMY FOREIGN SCI & TECH CENTER ATTN: DRXST-SD 220 7TH STREET, N.E. CHARLOTTESVILLE, VA 22901	1

NOTE: PLEASE NOTIFY COMMANDER, ARMAMENT RESEARCH, DEVELOPMENT, AND ENGINEERING CENTER, BENÉT LABORATORIES, CCAC, U.S. ARMY TANK-AUTOMOTIVE AND ARMAMENTS COMMAND, AMSTA-AR-CCB-O, WATERVLIET, NY 12189-4050 OF ADDRESS CHANGES.